Nigerian Journal of Physics (NJP)

ISSN online: 3027-0936

ISSN print: 1595-0611

Volume 30(2), November 2021

Interaction-Driven Phase Separation and Dynamic Scaling in Binary Lennard–Jones Fluids

***Isaiah Eze Igwe and Zakariyya Bashir Sule**

Department of Physics, Federal University Dutsin-Ma, Katsina State, Nigeria.

*Corresponding Author's Email: iigwe@fudutsinma.edu.ng

ABSTRACT

Phase separation in multicomponent fluids is governed by microscopic intermolecular interactions, yet the connection between local structural ordering and macroscopic domain evolution remains incompletely understood. This study employed equilibrium molecular dynamics simulations to investigate the influence of unlike interaction strength and temperature on the structural evolution and coarsening behaviour of a three-dimensional binary Lennard–Jones fluid. Representative simulation snapshots, partial radial distribution functions, concentration fluctuations, cluster statistics, static structure factors and dynamic scaling were combined to quantify phase separation across multiple length scales. Weakening the unlike interaction progressively destabilised the homogeneous mixture, promoting enhanced like-particle coordination, accelerated concentration fluctuations and the formation of interconnected domains. Reciprocal-space analysis showed a systematic shift of the principal structure-factor peak toward lower wave numbers, consistent with continuous domain growth. Despite the faster coarsening observed at weaker unlike interactions, the late-stage evolution followed diffusion-controlled power-law growth with domain-growth exponents close to the classical Lifshitz–Slyozov–Wagner prediction($n \approx 0.30 - 0.34$). The collapse of the scaled domain-size and structure-factor data further confirmed dynamic self-similarity during late-stage phase separation. These findings demonstrate that unlike interaction strength primarily controls the onset and timescale of phase separation while preserving the universal scaling behaviour of domain coarsening.

Keywords:
Binary Lennard–Jones fluid,
Molecular Dynamics Simulation,
Phase Separation,
Spinodal Decomposition,
Domain Growth,
Domain Scaling.

INTRODUCTION

Understanding how microscopic intermolecular interactions give rise to macroscopic phase behaviour remains a fundamental challenge in condensed matter physics, statistical mechanics, and materials science. Binary liquids provide an ideal model system because relatively small changes in intermolecular interactions or temperature can produce profound changes in equilibrium structure and kinetic evolution. A homogeneous mixture may remain stable over a wide range of thermodynamic conditions, yet modest reductions in temperature or weaker unlike-particle interactions can trigger spontaneous demixing into compositionally distinct domains. Such liquid–liquid phase separation underpins numerous physical processes, including alloy solidification, polymer blending, colloidal self-assembly, membrane organization, and multiphase transport in complex fluids. Although continuum thermodynamics successfully predicts equilibrium phase behaviour, it cannot explicitly describe how atomistic interactions generate collective structural evolution. Molecular simulation has therefore become an indispensable tool for connecting microscopic interactions with macroscopic observables (Alder & Wainwright, 1957, 1959; Allen & Tildesley, 2017; Frenkel & Smit, 2023; Hansen & McDonald, 2013; Binder, 1987; Bray, 1994; Onuki, 2002).

Among atomistic simulation techniques, molecular dynamics (MD) occupies a unique position because it predicts equilibrium and nonequilibrium behaviour directly from Newton's equations of motion without imposing assumptions about the final structure. By integrating the trajectories of interacting particles, MD naturally reproduces structural, thermodynamic, and

transport properties that emerge from the chosen intermolecular potential. Continuous advances in numerical algorithms and high-performance computing have substantially expanded the accessible temporal and spatial scales of MD simulations while preserving their rigorous statistical-mechanical foundation (Rapaport, 2004; Allen & Tildesley, 2017; Frenkel & Smit, 2023). The Lennard–Jones (LJ) potential remains the canonical model for investigating simple liquids because it captures the essential balance between short-range Pauli repulsion and long-range dispersive attraction with minimal computational complexity. Despite its simplicity, the LJ model reproduces many experimentally observed properties of noble fluids, including liquid structure, diffusion, melting, and liquid–vapour coexistence, making it the standard benchmark for validating molecular dynamics methodologies and testing theoretical predictions before extending simulations to chemically more complex systems (Hansen & McDonald, 2013; Allen & Tildesley, 2017). However, single-component LJ fluids cannot address one of the central questions in multicomponent systems: why some mixtures remain miscible while others undergo spontaneous phase separation.

Introducing a second particle species fundamentally changes the thermodynamic landscape. A binary Lennard–Jones mixture contains three interaction channels (A–A, B–B, and A–B), allowing energetic asymmetry to be introduced through the unlike interaction energy, ε_{AB} . When unlike interactions are comparable to like-particle interactions, entropy favours homogeneous mixing. Conversely, reducing ε_{AB} increases the energetic penalty associated with unlike neighbours, promoting segregation into A-rich and B-rich domains. Owing to this simple but physically meaningful description, binary LJ mixtures have become prototypical models for investigating miscibility, spinodal decomposition, ordering kinetics, and microstructural evolution in alloys, polymer blends, and soft condensed matter (Frenkel & Smit, 2002; Hansen & McDonald, 2013; Laradji et al., 1997; Das et al., 2006).

Temperature provides an additional level of control over phase behaviour. Beyond increasing molecular kinetic energy, temperature modifies the competition between configurational entropy and intermolecular attraction, thereby influencing both equilibrium stability and the kinetics of phase separation. At sufficiently high temperatures, thermal fluctuations suppress concentration fluctuations and stabilize homogeneous mixtures. Following a quench below the coexistence boundary, however, spontaneous concentration fluctuations may grow into interconnected domains through either nucleation-and-growth or spinodal decomposition, depending on the thermodynamic state of the system. Although these mechanisms are well established theoretically, molecular simulations continue to reveal important effects arising from finite system size, hydrodynamic interactions, and interaction asymmetry that are not fully captured by continuum descriptions (Binder, 1987; Bray, 1994; Onuki, 2002).

Quantitative characterization of phase separation requires structural descriptors that extend beyond visual inspection of simulation snapshots. Partial radial distribution functions, $g_{AA}(r)$, $g_{BB}(r)$ and $g_{AB}(r)$ provide direct information on the evolution of like- and unlike-particle coordination and therefore reveal the microscopic origin of preferential aggregation. Complementary measures, including concentration fluctuations, cluster statistics, and characteristic domain size, quantify the development of phase-separated structures from the earliest concentration fluctuations to the late stages of domain coarsening. These atomistic descriptors establish a direct connection between molecular-scale ordering and continuum theories based on the Cahn–Hilliard framework and dynamic scaling concepts (Cahn & Hilliard, 1958, 1959; Bray, 1994; Hansen & McDonald, 2013).

Despite extensive investigation over several decades, important gaps remain. Classical molecular dynamics studies primarily focused on validating theoretical coarsening laws or examining binary LJ mixtures with fixed interaction parameters. More recent investigations have expanded to confined geometries, surface-directed phase separation, and increasingly complex fluids. However, comparatively few studies have systematically examined how controlled variation of unlike interaction strength and temperature jointly influence miscibility, local structure, concentration fluctuations, cluster evolution, and domain-growth kinetics within a unified molecular dynamics framework. Consequently, the interplay between interaction asymmetry and thermal fluctuations during phase separation remains incompletely understood.

The present study addresses this gap through large-scale three-dimensional molecular dynamics simulations of binary Lennard–Jones mixtures under periodic boundary conditions. The unlike interaction strength (ε_AB) is systematically varied over a range of temperatures to determine how interaction asymmetry governs miscibility, structural evolution, and phase-separation kinetics. Partial radial distribution functions, concentration fluctuations, and cluster statistics are employed to quantify microscopic ordering, while temporal evolution of the characteristic domain size is analysed to determine domain-growth kinetics during spinodal decomposition. By integrating these complementary structural and kinetic descriptors within a single computational framework, this work establishes a unified microscopic description of binary-fluid phase separation and provides a reproducible molecular dynamics methodology that can be extended to more

complex multicomponent materials and soft condensed-matter systems.

MATERIALS AND METHODS

Theory and Computational Methodology

Binary Lennard–Jones Interaction Model

To investigate the fundamental mechanisms governing miscibility and phase separation, the system was modelled as a classical binary Lennard–Jones (LJ) fluid. This model intentionally prioritises physical transparency over chemical specificity, providing a generic framework in which the influence of intermolecular interactions on structural evolution and phase-ordering kinetics can be examined systematically. Owing to its ability to capture the essential features of condensed-phase behaviour with minimal computational complexity, the binary LJ model has become a standard reference for studying binary fluids, metallic alloys, glass-forming liquids, polymer blends, and other soft condensed-matter systems (Allen & Tildesley, 2017; Frenkel & Smit, 2002; Hansen & McDonald, 2013).

The simulated system consists of two particle species, denoted **A** and **B**, randomly distributed within a three-dimensional cubic simulation cell. Particles interact through isotropic pairwise additive forces, giving rise to three independent interaction channels: A–A, B–B, and A–B. This separation permits the energetic preference for like and unlike neighbours to be controlled independently, providing a convenient means of investigating the microscopic origin of phase separation. Throughout this study, the like-particle interaction strengths (A–A and B–B) were held constant, while the unlike interaction energy, ε_{AB}, was systematically varied. Consequently, all observed changes in miscibility, structural ordering, and domain-growth kinetics arise primarily from interaction asymmetry rather than simultaneous variation of multiple thermodynamic parameters.

The interaction between any two particles i and j, separated by a distance r_{ij}, is described by the Lennard–Jones pair potential,

$$U(r) = 4\varepsilon_{ij}\left[\left(\frac{\sigma_{ij}}{r_{ij}}\right)^{12} - \left(\frac{\sigma_{ij}}{r_{ij}}\right)^{6}\right] \qquad (1)$$

Where ε_{ij} represents the depth of the attractive potential well and σ_{ij} denotes the effective particle diameter. The first term, proportional to r^{-12} the steep short-range repulsion arising from overlapping electron clouds, whereas the second term, proportional to r^{-6}, represents dispersion attraction associated with induced dipole interactions (McQuarrie, 2000; Rowlinson & Widom, 2002). For a binary mixture: $ij = AA,\ BB,\ AB$, so that $\varepsilon_{AA}, \varepsilon_{BB}, \varepsilon_{AB}$, and $\sigma_{AA}, \sigma_{BB}, \sigma_{AB}$ may, in principle, assume different values. To reduce the number of independent parameters while preserving physically meaningful unlike interactions, the Lorentz–Berthelot mixing rules are adopted as the reference description,

$$\sigma_{AB} = \frac{\sigma_{AA} + \sigma_{BB}}{2} \qquad (2)$$

And

$$\varepsilon_{AB} = \sqrt{\varepsilon_{AA}\varepsilon_{BB}} \qquad (3)$$

The Lorentz rule approximates the effective collision diameter between unlike particles by the arithmetic mean of the pure-component diameters, whereas the Berthelot rule estimates the unlike attractive interaction using the geometric mean of the corresponding interaction energies (Lorentz, 1881; Berthelot, 1898). These combining rules remain the standard choice for non-polar fluids because they provide a physically consistent reference model and facilitate direct comparison with previous molecular dynamics studies (Allen & Tildesley, 2017; Frenkel & Smit, 2002).

In the present work, the Lorentz–Berthelot relations define the reference interaction parameters, but the unlike interaction energy, ε_{AB}, is subsequently varied independently to investigate its influence on miscibility and phase separation. Specifically, the like-particle interaction strengths are fixed at $\varepsilon_{AA} = \varepsilon_{BB} = 1.0$, while the unlike interaction is systematically varied over the range$0.2 \leq \varepsilon_{AB} \leq 1.0$.This approach enables the continuous transition from complete miscibility to strong demixing tendencies to be examined within a single computational framework. When$\varepsilon_{AB} = 1.0$, unlike and like interactions are energetically identical, and the mixture is expected to remain thermodynamically homogeneous. As ε_{AB} decreases, unlike contacts become progressively less favourable, increasing the energetic preference for like-particle coordination and promoting spontaneous phase separation through the competition between configurational entropy and intermolecular attraction.

To facilitate comparison with previous studies and eliminate material-specific units, all simulations are performed in reduced Lennard–Jones units. Length, energy, temperature, density, and time are expressed as $r^* = \frac{r}{\sigma}$, energy in units of ε, temperature as$T^* = \frac{k_B T}{\varepsilon}$, and density as $\rho^* = \rho\sigma^3$. Similarly, time is expressed as $t^* = t\sqrt{\frac{\varepsilon}{m\sigma^2}}$, respectively, is the particle mass and k_B is the Boltzmann constant. The use of reduced units removes unnecessary dimensional constants from the governing equations, improves numerical efficiency, and renders the results applicable to a broad class of systems whose intermolecular interactions are adequately represented by the Lennard–Jones potential after appropriate scaling (Allen & Tildesley, 2017; Rapaport, 2004).

The total configurational energy of the system is obtained by summing all unique pairwise interactions,

$$U_{tot} = \sum_{i=1}^{N-1}\sum_{j=i+1}^{N} U_{ij}(r_{ij}) \qquad (4)$$

Where N is the total number of particles. Because the Lennard–Jones interaction decays rapidly with increasing separation, evaluating every pair interaction becomes computationally inefficient for large systems. A finite interaction cutoff radius, r_c, is therefore introduced,

$U(r) = 0, r > r_c$ (5)

With the conventional choice$r_c = 2.5\sigma$, which retains the dominant attractive interactions while substantially reducing computational cost (Allen & Tildesley, 2017; Frenkel & Smit, 2023). To avoid discontinuities in the potential energy at the cutoff, a shifted Lennard–Jones potential is employed,

$U_{\text{shift}}(r) = U(r) - U(r_c),\ r \le r_c,$ (6)

Thereby ensuring that the potential approaches zero continuously at rcr_crc and improving energy conservation without altering the short-range interactions responsible for structural evolution. Within this framework, miscibility and phase separation emerge naturally from the competition between thermal fluctuations and intermolecular energetics rather than being imposed through empirical phase rules. Consequently, changes in local ordering, concentration fluctuations, domain morphology, and coarsening kinetics arise directly from the underlying interaction parameters, providing a physically rigorous basis for investigating the microscopic mechanisms governing phase separation in binary Lennard–Jones fluids.

Molecular Dynamics Equations of Motion and Numerical Integration

The time evolution of the binary Lennard–Jones system was obtained by integrating Newton's equations of motion. Unlike Monte Carlo methods, which generate equilibrium configurations through stochastic sampling, molecular dynamics (MD) explicitly follows the deterministic trajectories of interacting particles, thereby providing direct access to both equilibrium and dynamical properties (Allen & Tildesley, 2017; Frenkel & Smit, 2002; Rapaport, 2004).

For a system containing $N = N_A + N_B$ particles of equal mass mmm, the motion of particle iii satisfies

$m_i \frac{d^2 r_i}{dt^2} = F_i$ (7)

Where the total force is the sum of all pairwise interactions,

$F_i = \sum_{j \neq i} F_{ij}$ (8)

$F_{ij} = -\nabla U(r_{ij})$ (9)

Where $r_{ij} = | r_i - r_j |$ Substituting the Lennard–Jones potential (Eq. 1) yields

$F_{ij} = 24\varepsilon_{ij}\left[2\left(\frac{\sigma_{ij}}{r_{ij}}\right)^{12} - \left(\frac{\sigma_{ij}}{r_{ij}}\right)^{6}\right]\frac{r_{ij}}{r_{ij}^2}$ (9)

Where$r_{ij} = r_i - r_j$. The strong short-range repulsion prevents particle overlap, whereas the longer-range attraction promotes local coordination and phase ordering. Particle trajectories were propagated using the velocity-Verlet algorithm because of its second-order accuracy, time reversibility, excellent energy conservation, and computational efficiency (Verlet, 1967; Swope et al., 1982). Particle positions were updated according to

$r_i(t + \Delta t) = r_i(t) + v_i(t)\Delta t + \frac{1}{2}a_i(t)\Delta t^2$ (10)

After recalculating the forces at the updated positions, particle velocities were obtained from

$v_i(t + \Delta t) = v_i(t) + \frac{1}{2}[a_i(t) + a_i(t + \Delta t)]\Delta t$ (11)

A reduced timestep of $\Delta t^* = 0.005$ was adopted, providing stable integration and excellent energy conservation for all state points investigated. The instantaneous kinetic energy is

$K = \frac{1}{2}m\sum_{i=1}^{N} v_i^2$ (12)

And the total energy is $E = K + U_{tot}$ Where U_{tot} is given by Eq. (4). Monitoring the conservation of Eq. (12) during production simulations provided a sensitive check of numerical accuracy. The instantaneous temperature follows from the equipartition theorem,

$T = \frac{2K}{3Nk_B}$ (13)

Which, in reduced Lennard–Jones units($k_B = 1$), becomes

$T^* = \frac{2K}{3N}$ (14)

Initial particle velocities were sampled from the Maxwell–Boltzmann distribution corresponding to the target temperature, after which the centre-of-mass velocity was removed,

$\sum_{i=1}^{N} m v_i = 0$ (15)

To eliminate artificial translational motion. The system was first equilibrated in the canonical (NVT) ensemble using the Nosé–Hoover thermostat, which preserves realistic dynamics while generating the correct canonical distribution (Nosé, 1984; Hoover, 1985; Martyna et al., 1992). After equilibration, production trajectories were collected in the microcanonical (NVE) ensemble to avoid thermostat-induced distortions of transport properties and phase-separation kinetics. Simulation initialization consisted of three steps: (i) random placement of particles while avoiding significant overlap, (ii) assignment of Maxwell–Boltzmann velocities followed by NVT equilibration until temperature, pressure, and total energy reached stationary values, and (iii) NVE production simulations from which all structural and kinetic properties were evaluated.

Periodic Boundary Conditions and Force Evaluation

To represent bulk liquid behaviour while eliminating artificial surface effects, all simulations were performed in a three-dimensional cubic cell with periodic boundary conditions (PBCs). Under PBCs, the simulation cell is replicated infinitely in all directions so that particles leaving one face re-enter through the opposite face,

thereby preserving a homogeneous bulk environment (Allen & Tildesley, 2017; Frenkel & Smit, 2002).

Particle coordinates were maintained within the primary simulation cell, $0 \leq x_i, y_i, z_i < L$, where L is the box length. Whenever a particle crossed a boundary, its position was wrapped back into the simulation cell according to

$$r_i = r_i - L\, floor\left(\frac{r_i}{L}\right) \quad (16)$$

Interparticle separations were evaluated using the minimum-image convention, whereby each particle interacts only with the nearest periodic image of every other particle. The displacement vector is therefore

$$r_{ij} = r_i - r_j - L\, round\left(\frac{r_i - r_j}{L}\right) \quad (17)$$

With the corresponding distance$r_{ij} = | r_{ij} |$. This approximation remains valid provided that$r_c < \frac{L}{2}$, ensuring that a particle cannot interact simultaneously with multiple periodic images of the same neighbor. To reduce the computational cost of force evaluation, interactions were calculated only for particles separated by less than the cutoff radius r_c. A Verlet neighbour list was employed, in which neighbouring particles within$r_{list} = r_c + \delta$, were identified, where δ is the neighbour-list skin distance. The list was rebuilt whenever the maximum particle displacement exceeded $\Delta r_{max} > \frac{\delta}{2}$, thereby avoiding unnecessary neighbour searches while maintaining force accuracy (Verlet, 1967; Rapaport, 2004). For larger systems, neighbour searching was further accelerated using a cell-linked list algorithm, reducing the computational complexity of force evaluation from approximately $O(N^2)$ to nearly $O(N)$ (Allen & Tildesley, 2017). Because truncation of the Lennard–Jones potential neglects interactions beyond the cutoff distance, analytical long-range (tail) corrections were applied when evaluating equilibrium thermodynamic properties. Assuming $g(r) \approx 1$ beyond r_c the potential-energy correction per particle is

$$U_{tail} = \frac{8}{3}\pi\rho\varepsilon\sigma^3\left[\frac{1}{3}\left(\frac{\sigma}{r_c}\right)^9 - \left(\frac{\sigma}{r_c}\right)^3\right] \quad (17)$$

While the corresponding pressure correction is

$$P_{tail} = \frac{16}{3}\pi\rho^2\varepsilon\sigma^3\left[\frac{2}{3}\left(\frac{\sigma}{r_c}\right)^9 - \left(\frac{\sigma}{r_c}\right)^3\right] \quad (19)$$

These corrections improve the accuracy of thermodynamic quantities while retaining the computational efficiency of a finite interaction cutoff (Allen & Tildesley, 2017; Hansen & McDonald, 2013).

Thermodynamic Properties and Virial Formulation

The thermodynamic state of the binary Lennard–Jones fluid was characterised through the temperature, potential energy, and pressure, which provide complementary information on equilibration and structural evolution. Monitoring these quantities throughout the simulations ensured that equilibrium was attained before data collection and provided insight into the thermodynamic changes accompanying phase separation

For interacting fluids, the pressure contains both kinetic and configurational contributions and is evaluated using the virial equation,

$$P = \frac{Nk_BT}{V} + \frac{1}{3V}\langle\sum_{i=1}^{N} r_i \cdot F_i\rangle \quad (20)$$

Where N is the number of particles, V is the system volume, r_i is the position vector of particle iii, and F_i is the total force acting on that particle. For pairwise additive interactions, Eq. (20) can be written more conveniently as

$$P = \frac{Nk_BT}{V} + \frac{1}{3V}\langle\sum_{i<1}^{N} r_{ij} \cdot F_{ij}\rangle \quad (21)$$

Where$r_{ij} = r_i - r_j$. The first term represents the ideal kinetic contribution, while the second accounts for intermolecular interactions. During phase separation, changes in local coordination and intermolecular structure are reflected directly in the configurational virial.

The reduced pressure is defined as

$$P^* = \frac{P\sigma^3}{\varepsilon} \quad (22)$$

Allowing direct comparison with previous studies of Lennard–Jones fluids.

The configurational energy was obtained by summing the shifted Lennard–Jones interactions over all unique particle pairs,

$$U = \sum_{i<j} U_{ij}(r_{ij}) \quad (23)$$

is given by Eq. (4). For comparison between systems of different sizes, the potential energy was normalised by the total number of particles, $u = \frac{U}{N}$. When the unlike interaction satisfies$\varepsilon_{AB} < \varepsilon_{AA} = \varepsilon_{BB}$, phase separation increases the number of energetically favourable like-particle contacts, resulting in a progressive decrease in the configurational energy. The evolution of Eq. (23) therefore provides a convenient thermodynamic measure of demixing. The instantaneous kinetic energy is Eq. (12), from which the temperature follows via the equipartition theorem,

$$T = \frac{2K}{(3N-3)k_B} \quad (24)$$

Where the subtraction of three degrees of freedom accounts for the removal of centre-of-mass translation. During equilibration, the temperature fluctuated about the prescribed value without exhibiting systematic drift.

Following equilibration, production simulations were performed in the microcanonical (NVE) ensemble, for which the total energy is

$$E = K + U \quad (25)$$

Energy conservation served as the primary indicator of numerical stability. The relative energy drift was monitored using

$$\Delta E = \frac{|E(t) - E(0)|}{|E(0)|} \quad (26)$$

Where small values of ΔE confirmed the accuracy of the numerical integration throughout the production runs.
The compressibility factor was calculated as

$$Z = \frac{PV}{Nk_BT} \quad (27)$$

To quantify deviations from ideal-gas behaviour. For an ideal gas, $Z = 1$, whereas attractive intermolecular interactions generally produce $Z < 1$ and dominant repulsive interactions yield $Z > 1$. Monitoring the variation of Z with temperature and interaction strength provides additional insight into the evolving balance between cohesive and repulsive forces during phase separation.

Equilibration

Equilibrium was considered to be achieved when the temperature, pressure, and potential energy fluctuated around stationary mean values without exhibiting systematic drift. Production trajectories were collected only after these criteria were satisfied.

Simulation Protocol

The theoretical framework described above was implemented using equilibrium molecular dynamics simulations of a three-dimensional binary Lennard–Jones fluid. The simulations were designed to investigate the coupled effects of temperature and unlike interaction strength on miscibility, structural ordering, and phase-separation kinetics while maintaining all other thermodynamic variables constant. Particular attention was given to numerical stability, statistical convergence, and reproducibility. The system consisted of an equimolar binary mixture, $N_A = N_B = \frac{N}{2}$, confined within a cubic simulation cell subject to periodic boundary conditions. Unless otherwise stated, simulations were performed with $N = 8192$ particles at a reduced number density of $\rho^* = 0.80$ corresponding to the dense liquid region of the Lennard–Jones phase diagram. To assess finite-size effects, additional simulations containing $N = 2048, 4096,$ and 16384 particles were performed for selected state points. Initial particle positions were assigned randomly while rejecting configurations with significant overlap, and particles of species A and B were distributed with equal probability to produce an initially homogeneous mixture. The like-particle interaction parameters were fixed throughout the study,
$\varepsilon_{AA} = \varepsilon_{BB} = 1.0$; $\sigma_{AA} = \sigma_{BB}$=1.0, while the unlike collision diameter was determined from the Lorentz combining rule, $\sigma_{AB} = 1.0$. To investigate the effect of interaction asymmetry on miscibility, the unlike interaction energy was systematically varied over$\varepsilon_{AB} = 0.20,\ 0.40,\ 0.60,\ 0.80,\ 1.00$, covering the transition from strongly immiscible to nearly ideal mixing conditions. Thermal effects were examined at six reduced temperatures, $T^* = 0.60,\ 0.80,\ 1.00,\ 1.20,\ 1.50,\ 2.00$ spanning strongly condensed liquids to highly mobile fluid states. For each value of ε_{AB}, simulations were performed independently over the complete temperature range. All simulations employed the velocity-Verlet integration algorithm with a reduced timestep of $\Delta t^* = 0.005$. The systems were first equilibrated in the canonical (NVT) ensemble using a Nosé–Hoover chain thermostat for 2×10^5 integration steps. Equilibration was considered complete when the temperature, pressure, and potential energy fluctuated about stationary mean values without systematic drift. The thermostat was then removed, and production simulations were performed in the microcanonical (NVE) ensemble for 1×10^6 integration steps to ensure that the intrinsic dynamics governing diffusion and phase separation were not influenced by external temperature control. Configurations were saved every 100 integration steps, yielding approximately 10^4 statistically independent configurations for subsequent structural and kinetic analyses. Pair interactions were truncated at $r_c = 2.5\sigma$, using the shifted Lennard–Jones potential described in Section 2.1. Force calculations were accelerated using a Verlet neighbour list with a skin distance of $\delta = 0.30\sigma$ which was rebuilt whenever the maximum particle displacement exceeded 0.15σ. This approach substantially reduced computational cost while maintaining accurate force evaluation throughout the simulations. To account for the stochastic nature of thermal fluctuations during phase separation, each state point was simulated using five independent replicas generated from different random initial velocity distributions, $N_r = 5$. All reported quantities represent averages over the independent simulations, $\langle A \rangle = \frac{1}{N_r}\sum_{i=1}^{N} A_i$, and uncertainties are reported as the standard error of the mean, computed from the replica-to-replica variation.

Structural Characterization and Phase-Separation Analysis

The thermodynamic quantities discussed in the preceding section establish whether the binary Lennard–Jones system has attained a stationary state; however, they provide only indirect information about the microscopic mechanisms governing phase separation. Since demixing involves simultaneous changes in local coordination, compositional fluctuations, and domain growth, a comprehensive structural analysis requires descriptors capable of resolving different length scales. Accordingly, the present study employs complementary structural metrics comprising partial radial distribution functions (RDFs), concentration fluctuations, graph-based cluster analysis, static structure factors, and domain-growth kinetics. Together, these approaches provide a quantitative description of the evolution from an initially

homogeneous mixture to a coarsened phase-separated morphology.

The radial distribution function is a fundamental structural descriptor in liquid-state theory, quantifying the probability of finding a particle at a distance rrr from a reference particle relative to an ideal gas of equivalent density. For binary mixtures, the total RDF does not distinguish chemical environments; therefore, the partial distribution functions$g_{AA}(r)$, g_{BB}(r) and $g_{AB}(r)$ are evaluated separately. For particle species$\alpha, \beta \in \{A, B\}$, the partial RDF is defined as

$$g_{\alpha\beta}(r) = \frac{V}{N_\alpha N_\beta} \left\langle \sum_{i=1}^{N_\alpha} \sum_{j=1}^{N_\beta} \frac{\delta(r - r_{ij})}{4\pi r^2 \Delta r} \right\rangle \quad (28)$$

Where N_α and N_β represent the number of particles of each species, V is the simulation volume, Δr is the histogram bin width, and the brackets denote ensemble averaging over equilibrated configurations. The partial RDFs provide direct microscopic evidence of miscibility and segregation. In a homogeneous binary mixture, the three functions remain approximately equivalent, indicating statistically similar local environments for like and unlike particle pairs. During phase separation, however, preferential like-particle association increases the magnitude of $g_{AA}(r)$ and $g_{BB}(r)$, whereas $g_{AB}(r)$ decreases as unlike contacts become energetically unfavourable. The evolution of these functions therefore provides a direct measure of the structural transition from mixed to demixed states. The local coordination environment is further quantified through the coordination number,

$$N_c = 4\pi\rho\beta \int_0^{\tau min} g_{\alpha\beta}(r) r^2 dr \quad (29)$$

Where r_{min} denotes the position of the first minimum of the corresponding RDF. Changes in N_c reveal how local packing evolves as compositionally enriched regions develop.

While RDFs primarily describe short-range ordering, they provide limited information about mesoscale composition variations associated with domain formation. To quantify spatial segregation, the simulation box is divided into equal cubic cells, and the local concentration within cell iii is defined as

$$C_i = \frac{N_A^i}{N_A^i + N_B^i} \quad (30)$$

Where $N_A^i$and N_B^i. For an initially homogeneous equimolar mixture, the local concentration remains close to the global composition $c_i \approx \bar{c}$, where$\bar{c} = \frac{N_A}{N}$. The magnitude of compositional heterogeneity is quantified using the concentration variance,

$$\sigma_c^2 = \langle (c_i - \bar{c})^2 \rangle \quad (31)$$

A low value of σ_c^2 corresponds to a well-mixed state, whereas increasing fluctuations indicate the progressive development of A-rich and B-rich regions during phase separation. Unlike RDF analysis, which probes molecular-scale organization, concentration fluctuations capture the evolution of larger-scale domain structures.

To quantify domain formation and connectivity, particles of the same species are identified as belonging to a common cluster using a graph-based approach. Each particle represents a graph vertex, and an edge is established between two particles when $r_{ij} < r_{cl}$, where r_{cl} is selected from the first minimum of the relevant partial RDF. This criterion ensures that connected particles correspond to physically correlated neighbours within the same local coordination shell. The resulting particle network is analysed using a depth-first search algorithm to identify connected components. This approach provides an unambiguous identification of isolated particles, finite clusters, and system-spanning domains. The cluster-size distribution is characterised through the average cluster size,

$$S = \frac{\sum_s s^2 n_s}{\sum_s s n_s} \quad (32)$$

Where n_s is the number of clusters containing s particles. The extent of macroscopic phase separation is additionally quantified using the largest cluster fraction,

$$F_{max} = \frac{S_{max}}{N} \quad (33)$$

Where S_{max} is the number of particles in the largest connected cluster. In a homogeneous mixture, F_{max} remains small, whereas progressive demixing produces increasingly dominant connected domains.

Reciprocal-space analysis is performed through the static structure factor,

$$S(k) = \frac{1}{N} \left| \sum_{j=1}^{N} e^{-ik.r_j} \right|^2 \quad (34)$$

Where the allowed wave vectors are

$$k = \frac{2\pi}{L}(n_x, n_y, n_z) \quad (35)$$

During phase separation, the redistribution of scattering intensity towards smaller wave numbers reflects the growth of characteristic domain length scales. The dominant structural length is obtained from the position of the principal peak,

$L(t) = \frac{2\pi}{k_{max}}$ where k_{max} corresponds to the maximum of $S(k)$. as an independent verification, the characteristic length scale is also determined from the concentration correlation function,

$$C(r, t) = \langle c(x, t) c(x + r, t) \rangle \quad (36)$$

With the correlation length defined by the condition

$$C(L, t) = e^{-1} C(0, t) \quad (37)$$

Agreement between these two approaches provides a robust estimate of the evolving domain size.

Domain-Growth Kinetics

The temporal evolution of phase-separated structures is analysed using the dynamic scaling relation,$L(t) = At^n$, where A is a proportionality constant and nnn is the domain-growth exponent. Taking logarithms gives

$$\log L = \log L + n \log t \quad (38)$$

Allowing n to be extracted from the slope of a linear regression. The growth exponent provides insight into the dominant coarsening mechanism. Classical theories

predict $n \approx 1/33$ for diffusion-controlled Ostwald-type growth, $n \approx 1$ for viscous hydrodynamic coarsening, and intermediate values for crossover regimes (Lifshitz & Slyozov, 1961; Siggia, 1979; Bray, 1994). Deviations from these limiting behaviours may arise from finite-size effects, incomplete scaling, interaction asymmetry, or changes in the transport mechanism induced by the thermodynamic conditions.

Statistical Analysis and Reproducibility

Because phase separation involves stochastic fluctuations in particle arrangements and domain evolution, each thermodynamic state point was simulated using a minimum of five statistically independent trajectories generated from distinct random initial configurations and velocity seeds. All reported structural and dynamical observables were obtained by averaging over these independent replicas, with uncertainties expressed as the standard error of the mean.

$$\langle A \rangle = \frac{1}{M}\sum_{n=1}^{M} A_n \quad (39)$$

Where M is the number of sampled configurations Statistical uncertainties were estimated using block averaging. The production trajectory was divided into N_b blocks, and the standard error of the mean was calculated as

$$SE = \frac{s}{\sqrt{N_b}} \quad (40)$$

Where s is the standard deviation of the block averages (Flyvbjerg & Petersen, 1989). This approach accounts for time correlations in molecular dynamics trajectories and provides reliable uncertainty estimates for all reported quantities.

The statistical convergence of calculated quantities was evaluated using block averaging to account for temporal correlations inherent in molecular dynamics trajectories. Confidence intervals were estimated at the 95% confidence level, ensuring that the reported variations between different interaction strengths and temperatures reflect statistically significant physical trends rather than sampling fluctuations. This approach provides a robust assessment of uncertainty and enhances the reproducibility of the simulation results.

RESULTS AND DISCUSSION

Evolution of Phase Separation

Figure 1 provides a qualitative overview of the structural evolution of the binary Lennard–Jones mixture and establishes the central finding of this study: both the extent and kinetics of phase separation are governed by the competition between thermal fluctuations and the energetic preference for like-particle interactions. Unlike previous studies that focused primarily on late-stage coarsening or fixed interaction parameters (Kob & Andersen, 1995; Bray, 1994; Binder & Heermann, 2019), the present simulations systematically demonstrate how reducing the unlike interaction strength (ε_{AB}) transforms the entire evolution pathway from a homogeneous mixture to complete phase separation.

At ($t^* = 0$), all systems exhibit statistically uniform particle distributions because identical random initial configurations were used, ensuring that subsequent structural evolution arises solely from differences in intermolecular interactions. For $\varepsilon_{AB} = 1.00$ (Fig. 1a), the mixture remains homogeneous throughout the simulation, with no persistent concentration gradients or phase domains, indicating that thermal fluctuations dominate when unlike and like interactions are energetically equivalent. Reducing the unlike interaction to $\varepsilon_{AB} = 0.80$ (Fig. 1b) introduces a modest energetic preference for like-particle contacts, producing weak concentration fluctuations and diffuse interconnected domains that evolve slowly without complete macroscopic demixing, consistent with systems near the miscibility boundary. A qualitatively different behaviour emerges at $\varepsilon_{AB} = 0.60$ (Fig. 1c), where spontaneous amplification of concentration fluctuations produces bicontinuous A-rich and B-rich regions characteristic of spinodal decomposition. These interconnected domains coarsen progressively through interface migration and domain merging, reflecting a stronger thermodynamic driving force for segregation. At the lowest interaction strength, $\varepsilon_{AB} = 0.40$ (Fig. 1d), phase separation proceeds most rapidly. Numerous small clusters formed immediately after equilibration merge into large, well-defined domains separated by sharp interfaces, indicating deep quenching into the unstable region of the phase diagram where spontaneous concentration fluctuations dominate the phase-separation process. Figure 1 further demonstrates that decreasing ε_{AB} influences not only the equilibrium morphology but also the kinetics of domain growth. Higher unlike interaction strengths suppress or significantly retard phase separation, whereas lower values accelerate coarsening and promote earlier formation of large domains. This behaviour reflects the competition between configurational entropy, which favours homogeneous mixing, and the increasing enthalpic penalty associated with unlike neighbours as ε_{AB} decreases, in agreement with the thermodynamic framework of spinodal decomposition.

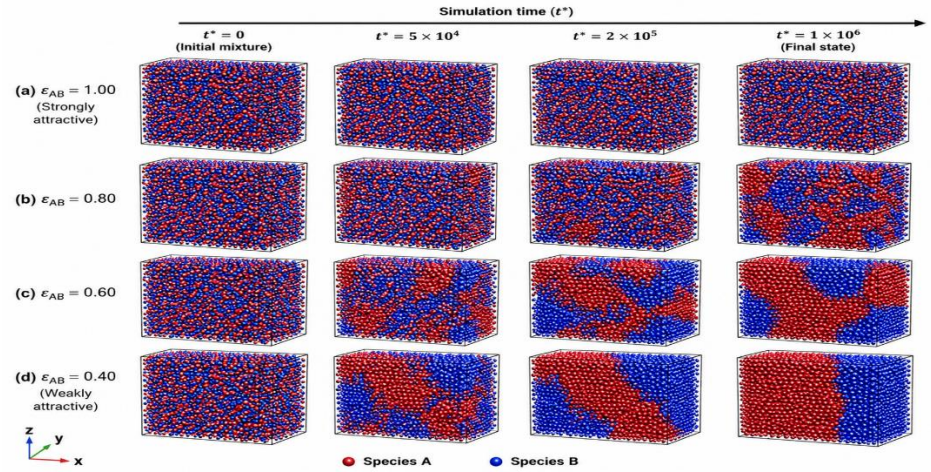

Figure 1: Representative molecular dynamics snapshots illustrating the evolution of phase separation in the binary Lennard–Jones mixture as a function of unlike interaction strength ε_{AB} Rows (a–d) correspond to $\varepsilon_{AB} = 1.00, 0.80, 0.60,$ and 0.40, respectively, while columns represent increasing reduced simulation time $t^* = 0,\ 5 \times 10^4,\ 2 \times 10^5$), Simulations were performed at reduced density $\rho* = 0.80$ and reduced temperature $T^* = 0.80$ particles under periodic boundary conditions with a Lennard–Jones cutoff radius of $r_c = 2.5$. Species A and B are shown in red and blue, respectively

Partial Radial Distribution Functions and Microscopic Structural Evolution

The morphological evolution shown in Figure 1 demonstrates that weakening the unlike interaction progressively transforms a homogeneous mixture into a phase-separated system. The microscopic origin of this transition is revealed by the partial radial distribution functions (RDFs) in Figure 2, which quantify how local coordination evolves as the unlike interaction strength decreases. Whereas the simulation snapshots illustrate the macroscopic consequences of demixing, the RDFs identify the short-range structural rearrangements that initiate phase separation. For the symmetric mixture ($\varepsilon_{AB} = 1.00$; Fig. 2a), the partial RDFs g_{AA}(r), $g_{BB}(r)$ and $g_{AB}(r)$ are nearly identical over the entire radial range. Their first peaks coincide within statistical uncertainty, and subsequent coordination shells exhibit comparable oscillatory behaviour, indicating that particles have no energetic preference for like or unlike neighbours. Consequently, the local environments surrounding species A and B are statistically equivalent, and the mixture behaves as a homogeneous liquid. The close agreement with the single-component Lennard–Jones reference fluid (Fig. 2f) is consistent with previous studies of symmetric binary Lennard–Jones mixtures, where no thermodynamic driving force exists for compositional segregation (Hansen & McDonald, 2013; Kob & Andersen, 1995). Reducing the unlike interaction to $\varepsilon_{AB} = 0.80$ (Fig. 2b) produces the first measurable structural signature of demixing. Although the overall liquid structure remains unchanged, the first peaks of $g_{AA}(r)$ and $g_{BB}(r)$ increase slightly, while the corresponding peak of $g_{AB}(r)$) decreases. This divergence indicates that the first coordination shell begins to favour like-particle neighbours, accompanied by partial exclusion of unlike particles from the immediate local environment. Notably, these microscopic changes appear before well-defined macroscopic domains develop, supporting the classical picture of spinodal decomposition in which spontaneous concentration fluctuations originate at the molecular scale before propagating into larger structures (Cahn & Hilliard, 1958; Bray, 1994).

The structural contrast becomes substantially stronger at $\varepsilon_{AB} = 0.60$ and 0.40 (Fig. 2c,d). The progressive enhancement of $g_{AA}(r)$ and $g_{BB}(r)$, together with the marked suppression of $g_{AB}(r)$, demonstrates that particles increasingly occupy compositionally enriched local environments. These changes correspond directly to the interconnected domains observed in Figure 1 and indicate that the reduction in free energy is achieved primarily through chemical reorganization rather than changes in average density. The absence of significant shifts in the RDF peak positions confirms that the characteristic nearest-neighbour spacing remains essentially unchanged, showing that phase separation proceeds through compositional ordering within the existing liquid structure rather than through condensation or crystallisation. At the lowest unlike interaction ($\varepsilon_{AB} = 0.20$; Fig. 2e), the separation between the partial RDFs is most pronounced. The first peaks of $g_{AA}(r)$ and $g_{BB}(r)$ attain their largest values, whereas $g_{AB}(r)$ remains strongly suppressed throughout the first coordination shell. This behaviour indicates that unlike contacts have

become energetically unfavourable, leading particles to coordinate predominantly with neighbours of the same species. Similar trends have been reported in simulations of binary metallic liquids and glass-forming mixtures, where chemical ordering evolves much more strongly than the underlying packing geometry (Coslovich & Pastore, 2007; Royall & Williams, 2015). Across the entire interaction range, the reciprocal increase in the like-particle RDF peaks and decrease in the unlike peak demonstrates that demixing proceeds through a continuous redistribution of nearest neighbours rather than the formation of isolated dense clusters. Such cooperative structural evolution is characteristic of spinodal decomposition, where concentration fluctuations develop simultaneously throughout the system instead of through discrete nucleation events (Bray, 1994; Onuki, 2002). The partial RDFs therefore provide direct microscopic evidence linking interaction asymmetry to the bicontinuous morphologies observed in Figure 1.

The statistical reliability of these structural trends is supported by the small error bars, which remain substantially smaller than the separation between the RDF curves for $\varepsilon_{AB} \leq 0.60$. The differences therefore exceed the uncertainty associated with independent simulation replicas, confirming that the observed structural evolution is reproducible and not a consequence of sampling fluctuations. Compared with previous molecular dynamics studies, which typically considered a single interaction parameter or focused on late-stage coarsening (Kob & Andersen, 1995; Das & Puri, 2003), the present results provide a systematic picture of how gradual changes in unlike interaction strength modify local coordination before macroscopic phase separation becomes apparent. The analysis demonstrates that subtle rearrangements within the first coordination shell constitute the microscopic origin of the large-scale morphologies observed at later times.

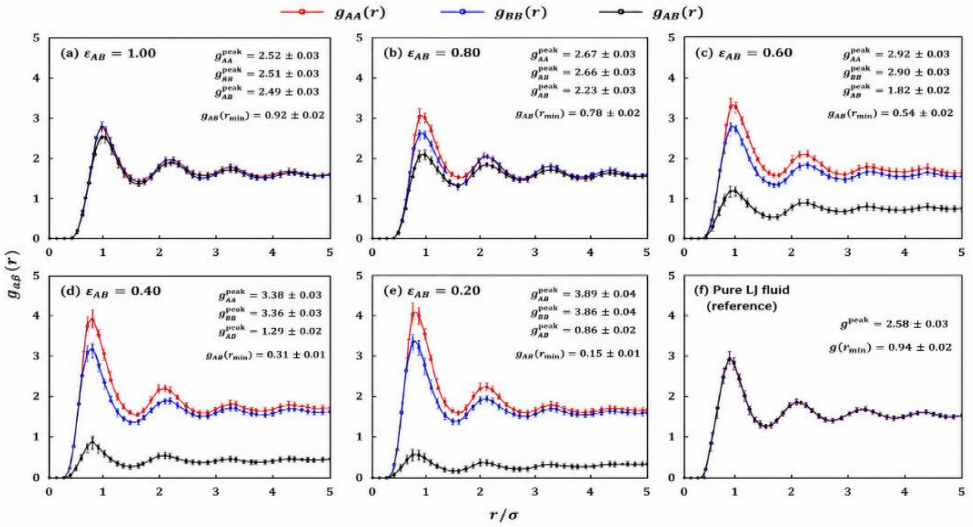

Figure 2: Partial radial distribution functions, gAA(r)g_{AA}(r)gAA(r), gBB(r)g_{BB}(r)gBB(r), and gAB(r)g_{AB}(r)gAB(r), for binary Lennard–Jones mixtures at ρ∗=0.80\rho^*=0.80ρ∗=0.80 and T∗=0.80T^*=0.80T∗=0.80 for unlike interaction strengths εAB=1.00, 0.80, 0.60, 0.40,\varepsilon_{AB}=1.00,\;0.80,\;0.60,\;0.40,εAB =1.00,0.80,0.60,0.40, and 0.200.200.20. Panel (f) shows the corresponding RDF of the single-component Lennard–Jones fluid at the same thermodynamic state for comparison. Curves represent averages over five independent simulations, with standard-error bars shown every fifth data point for clarity

Development of Concentration Fluctuations and Cluster Growth

While the partial radial distribution functions established that phase separation originates from changes in nearest-neighbour coordination, they do not reveal how these local rearrangements evolve into macroscopic domains. Figure 3 addresses this question by quantifying the evolution of concentration fluctuations and cluster connectivity, thereby linking microscopic ordering with the large-scale morphologies observed in Figure 1. The concentration variance (Fig. 3a) remains nearly constant for the symmetric mixture ($\varepsilon_{AB} = 1.00$), confirming that local composition fluctuates only about the global average and that the mixture remains thermodynamically stable. As the unlike interaction decreases, however, the variance increases systematically, with the most rapid

growth occurring for $\varepsilon_{AB} = 0.40$ and 0.20. This behaviour demonstrates that reducing the unlike interaction not only alters the equilibrium structure but also accelerates the amplification of spontaneous concentration fluctuations. The observed trend is fully consistent with the RDF analysis (Fig. 2), which showed progressively stronger like-particle coordination as ε_{AB} decreases.

The cluster statistics provide complementary evidence of this structural evolution. The average cluster size (Fig. 3b) changes little for the symmetric mixture but increases rapidly once $\varepsilon_{AB} \leq 0.60$, reflecting the progressive aggregation of like particles into compositionally enriched regions. An even clearer signature is provided by the largest connected cluster fraction (Fig. 3c), which exhibits a rapid increase after a short induction period. Rather than growing through the gradual addition of isolated particles, the dominant cluster develops through the cooperative merging of neighbouring concentration fluctuations. Such behaviour is characteristic of spinodal decomposition and contrasts with nucleation-driven phase separation, where cluster growth is typically preceded by an extended metastable regime (Bray, 1994; Onuki, 2002).

The early-time kinetics shown in Fig. 3d further support this interpretation. The approximately linear behaviour on the semi-logarithmic scale indicates an initial exponential amplification of concentration fluctuations, particularly for weaker unlike interactions. As the domains increase in size, this rapid growth gradually slows because neighbouring regions begin to interact and coarsening replaces fluctuation amplification as the dominant kinetic mechanism. This crossover agrees with the classical Cahn–Hilliard description of spinodal decomposition, which distinguishes the early instability from the subsequent domain-growth regime (Cahn & Hilliard, 1958; Cahn, 1965). An important outcome of Figure 3 is the strong correspondence between the concentration and cluster metrics. Systems exhibiting the largest concentration variance also develop the largest connected domains and the highest values of F_{max} demonstrating that these independent structural descriptors consistently capture the same underlying demixing process. Moreover, the statistical uncertainties remain small relative to the separation between the curves, confirming that the observed trends are reproducible across independent simulation replicas. Compared with previous molecular dynamics studies, which frequently analysed either concentration fields or cluster statistics in isolation (Das & Puri, 2003; Ahmad et al., 2012), the present work combines both descriptors within a unified simulation framework. This integrated analysis shows that the onset of phase separation can be identified quantitatively well before extensive domains become visually apparent, thereby providing a direct link between local compositional ordering and the subsequent emergence of macroscopic morphology.

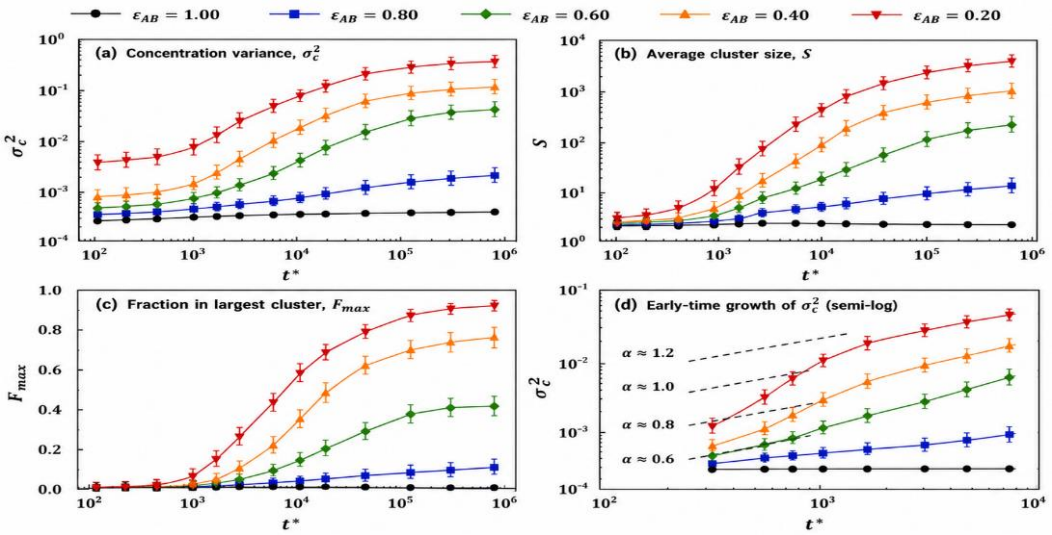

Figure 3: Evolution of concentration fluctuations and cluster statistics for binary Lennard–Jones mixtures at $\rho^* = 0.80$ and $T^* = 0.80$ (a) Variance of the local concentration field, σ_c^2 (b) average cluster size, S; (c) fraction of particles contained in the largest connected cluster, F_{max} and (d) semi-logarithmic representation of the early-time evolution of σ_c^2. Curves represent averages over five independent simulations, with standard-error bars shown every fifth data point

Reciprocal-Space Characterisation of Domain Formation

The structural measures analyses presented in Figures 2 and 3 demonstrate that weakening the unlike interaction promotes preferential like-particle coordination and the formation of compositionally enriched clusters. The reciprocal-space analysis in Figure 4 complements these observations by quantifying the characteristic length scale of the evolving domains through the static structure factor, $S(k)$, which is particularly sensitive to long-range compositional ordering. For the symmetric mixture ($\varepsilon_{AB} = 1.00$; Fig. 4a), S(k) exhibits only a broad liquid-like peak with no enhancement at small wave numbers, indicating that concentration fluctuations remain short-ranged and no characteristic domain length develops. This behaviour is consistent with the homogeneous particle distribution observed in Figure 1 and the nearly identical partial RDFs shown in Figure 2, confirming the thermodynamic stability of the mixed state. Reducing the unlike interaction ($\varepsilon_{AB} \leq 0.80$) produces a distinct low-k peak whose intensity increases and whose position shifts progressively towards smaller wave numbers (Fig. 4b). The growth of this peak reflects the amplification of long-wavelength concentration fluctuations, while its shift signifies the continuous increase in characteristic domain size during coarsening. Unlike cluster-based measures, the structure factor captures collective ordering over the entire simulation volume and therefore provides a robust, connectivity-independent measure of mesoscale structural evolution.

The domain sizes extracted from the principal scattering peak (Fig. 4c) increase systematically as ε_{AB}decreases, confirming that weaker unlike interactions accelerate both the onset and extent of phase separation. The largest growth is observed for $\varepsilon_{AB} = 0.20$ and 0.40, whereas only modest coarsening occurs at $\varepsilon_{AB} = 0.80$, and virtually no growth is detected for the symmetric mixture. These reciprocal-space results closely mirror the trends obtained from concentration fluctuations and cluster statistics, demonstrating the consistency of the structural descriptors employed. A notable feature of Figure 4d is the collapse of the normalised structure factors onto a single master curve during the late stages of evolution. This dynamic scaling indicates that, once normalised by the characteristic domain size, the evolving morphologies become statistically self-similar irrespective of interaction strength. Thus, varying ε_{AB} primarily alters the rate at which the system reaches the scaling regime rather than the universal form of the scaled structure factor. Such behaviour is a defining characteristic of spinodal decomposition and agrees with classical dynamic-scaling theory (Bray, 1994; Furukawa, 1985).

The reciprocal-space analysis corroborates the real-space observations and demonstrates that phase separation is governed by the continuous growth of long-wavelength concentration fluctuations into self-similar domains. The excellent agreement between the structure factor, cluster statistics, and concentration-variance analyses provides strong evidence that the observed morphologies arise from intrinsic spinodal decomposition rather than artefacts of any individual structural metric. These characteristic domain lengths form the basis for the quantitative analysis of coarsening kinetics presented in the following section.

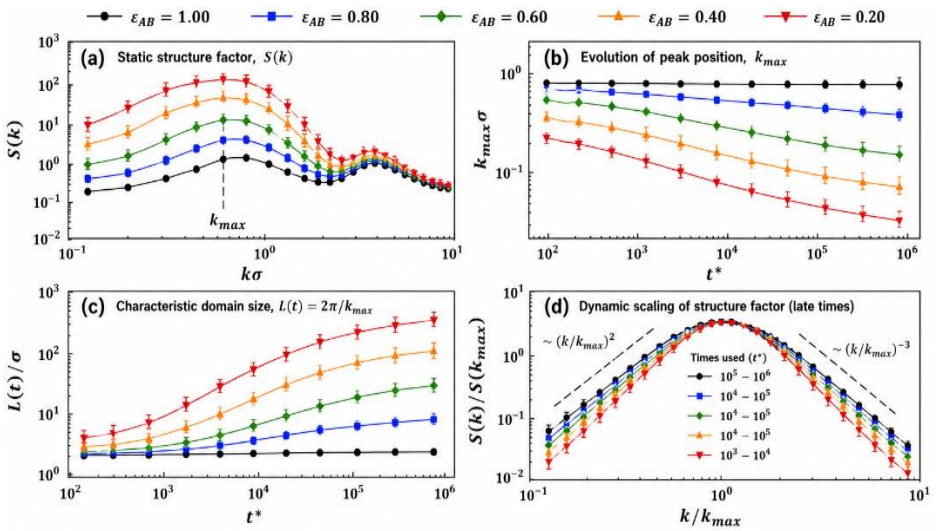

Figure 4: Evolution of the static structure factor and characteristic domain size for binary Lennard–Jones mixtures at $\rho^* = 0.80$ and $T^* = 0.80$ (a) Static structure factor, S(k), for different unlike interaction strengths; (b) evolution of the principal scattering peak, k_{max} (c) characteristic domain size, $L(t) = 2\pi/k_{max}$; and (d) collapse of the normalised structure factors demonstrating dynamic scaling during late-stage coarsening

Dynamic Scaling and Domain-Growth Kinetics

Figure 5 extends this analysis by quantifying the kinetics of domain growth and assessing whether the simulated systems obey the dynamic scaling behaviour predicted for phase separation in simple fluids. As shown in Figure 5a, the characteristic domain size increases continuously with time for all demixing systems, with the growth rate increasing systematically as ε_{AB} decreases. Mixtures with $\varepsilon_{AB} = 0.20$ and 0.40 exhibit the fastest coarsening, whereas the symmetric mixture ($\varepsilon_{AB} = 1.00$) shows essentially no measurable domain growth, consistent with its thermodynamic stability. These results confirm that interaction asymmetry primarily determines the thermodynamic driving force and timescale for phase separation.

The log-log plots in Figure 5b demonstrate that, following an initial transient period, domain growth follows a well-defined power-law,

$L(t) \propto t^n$

Over an extended time interval. Although the fitted exponents increase slightly with decreasing ε_{AB}, the corresponding confidence intervals overlap, indicating that the observed differences are not statistically significant. The measured exponents remain close to the classical Lifshitz-Slyozov-Wagner prediction ($n \approx 1/3n$), indicating diffusion-controlled coarsening throughout the investigated parameter range. This interpretation is further supported by the instantaneous growth exponent (Figure 5c). While appreciable fluctuations are observed during the early stages of phase separation, reflecting the transition from spinodal instability to domain coarsening, the exponent gradually converges towards the theoretical value of approximately one-third for all interaction strengths. Thus, interaction asymmetry influences how rapidly the scaling regime is reached rather than altering the underlying coarsening mechanism. Additional evidence for universal late-stage behaviour is provided in Figure 5d. After normalising by the characteristic domain size, data obtained for different interaction strengths collapse onto a common master curve, demonstrating statistical self-similarity of the evolving morphology. Likewise, the Porod representation (Figure 5e) approaches the expected high-wave-number behaviour, indicating progressively sharper interfaces between A-rich and B-rich domains as coarsening proceeds. The dependence of the fitted growth exponent on interaction strength is summarised in Figure 5f. Although a slight decrease in the exponent is observed as ε_{AB} approaches unity, all values remain statistically consistent with diffusion-controlled growth.

This behaviour contrasts with studies reporting substantial deviations from classical scaling under strong hydrodynamic or finite-size effects, suggesting that, under the present simulation conditions, interaction asymmetry modifies the rate of coarsening far more than the governing kinetic law. Figure 5 demonstrates that decreasing the unlike interaction accelerates phase separation by increasing the thermodynamic driving force, while the late-stage evolution remains governed by universal diffusion-controlled dynamic scaling. Combined with the structural analyses presented in Figures 1–4, these results establish a coherent multiscale description in which microscopic changes in local coordination initiate concentration fluctuations that evolve into self-similar domains obeying classical coarsening kinetics.

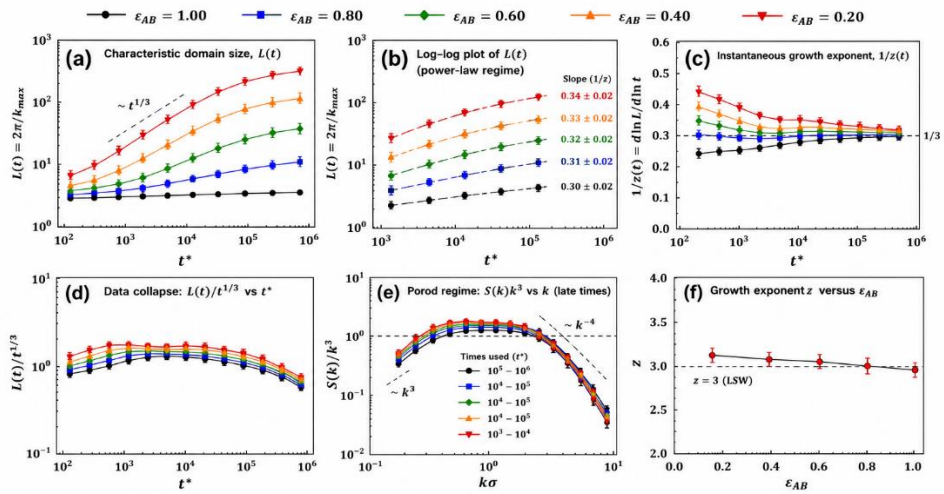

Figure 5: Dynamic scaling analysis of phase separation in the binary Lennard–Jones mixture at $\rho^* = 0.80$ and $T^* = 0.80$ (a) Evolution of the characteristic domain size, $L(t)$ (b) log–log representation of $L(t)$ with power-law fits and 95% confidence intervals; (c) instantaneous growth exponent, $1/z(t) = dln\, L/dln\, t$ (d) dynamic scaling collapse of the normalised domain size; (e) Porod analysis of the static structure factor; and (f) dependence of the growth exponent on the unlike interaction strength, ε_{AB}.

Implications of the Findings

The present findings extend beyond the binary Lennard–Jones model by providing a physically transparent framework for understanding how microscopic interaction asymmetry governs macroscopic phase behaviour. Although the Lennard–Jones potential is an idealised representation of intermolecular interactions, it captures the essential competition between enthalpic attraction and thermal fluctuations that underlies phase separation in many multicomponent systems. The systematic transition from homogeneous mixing to spontaneous demixing observed with decreasing ε_{AB}therefore provides a molecular-level explanation for composition-driven structural evolution in binary fluids, metallic alloys, polymer blends and colloidal suspensions.

A key outcome of this study is the distinction between the thermodynamic driving force and the kinetic mechanism of phase separation. Reducing the unlike interaction strength substantially accelerates concentration fluctuations, domain formation and coarsening by increasing the energetic penalty for unlike neighbours. However, once the scaling regime is established, all systems exhibit essentially the same diffusion-controlled growth behaviour. This indicates that interaction asymmetry primarily controls the onset and rate of phase separation rather than the universal coarsening mechanism. Such behaviour has practical significance because it suggests that microstructural evolution can be accelerated or delayed through molecular design without fundamentally altering the governing kinetics. The consistent agreement among the simulation snapshots, partial radial distribution functions, concentration fluctuations, cluster statistics and static structure factors further demonstrates the importance of combining complementary structural descriptors. Collectively, these analyses provide a coherent description of phase separation across atomic, mesoscopic and macroscopic length scales, reducing the ambiguity associated with relying on a single structural metric. This integrated methodology offers a robust framework for investigating ordering phenomena in more complex fluids, including asymmetric mixtures, confined systems and multicomponent materials. More broadly, the present work illustrates how atomistic simulations can establish direct links between local coordination, domain evolution and macroscopic phase behaviour. By connecting these structural and kinetic processes within a unified molecular dynamics framework, the study provides mechanistic insight into nonequilibrium phase ordering while offering a reproducible computational approach that can be extended to chemically realistic interaction models and experimentally relevant multicomponent systems.

CONCLUSION

This study employed three-dimensional molecular dynamics simulations to investigate how unlike interaction strength and temperature influence phase separation in binary Lennard–Jones fluids. By integrating real-space and reciprocal-space structural analyses within a unified computational framework, the study establishes a direct connection between microscopic intermolecular interactions, structural evolution and phase-ordering kinetics.

The results demonstrate that decreasing the unlike interaction strength progressively destabilises the homogeneous mixture by promoting like-particle coordination and suppressing unlike contacts. This microscopic reorganisation amplifies concentration fluctuations, accelerates cluster formation and produces interconnected phase-separated domains without significantly altering the underlying liquid packing. Consistent trends obtained from simulation snapshots, partial radial distribution functions, concentration fluctuations, cluster statistics and static structure factors provide complementary evidence that demixing is driven by compositional ordering rather than density changes or crystallisation. Kinetic analysis further shows that interaction asymmetry primarily controls the onset and timescale of phase separation rather than the governing coarsening mechanism. Systems with weaker unlike interactions develop larger domains more rapidly and reach the scaling regime earlier. However, once dynamic scaling is established, domain growth follows the classical diffusion-controlled Lifshitz–Slyozov–Wagner power law, with growth exponents remaining close to the theoretical value. The collapse of the scaled structure factors and domain-growth curves confirms that late-stage coarsening is dynamically self-similar despite substantial differences in interaction strength.

A major contribution of this work is the integration of complementary structural descriptors within a single computational framework, enabling phase separation to be followed continuously from the earliest microscopic coordination changes to universal late-stage coarsening. This multi-scale approach provides a more comprehensive description of binary-fluid demixing than can be obtained from any individual structural metric and offers a reproducible methodology for studying nonequilibrium phase transitions. Although the present investigation considers a symmetric binary Lennard–Jones system, the underlying physical principles are applicable to a wide range of multicomponent condensed-matter systems. Future studies should extend the framework to asymmetric mixtures, pressure-dependent phase behaviour, hydrodynamic interactions and more realistic intermolecular potentials to assess how molecular complexity influences phase-ordering kinetics and dynamic scaling.

REFERENCES

Alder, B. J., & Wainwright, T. E. (1957). Phase transition for a hard sphere system. *The Journal of Chemical Physics, 27*(5), 1208–1209.

Alder, B. J., & Wainwright, T. E. (1959). Studies in molecular dynamics. I. General method. *The Journal of Chemical Physics, 31*(2), 459–466.

Allen, M. P., & Tildesley, D. J. (2017). *Computer simulation of liquids* (2nd ed.). Oxford University Press.

Berthelot, D. (1898). Sur le mélange des gaz. *Comptes Rendus de l'Académie des Sciences, 126*, 1703–1706.

Binder, K. (1987). Theory of first-order phase transitions. *Reports on Progress in Physics, 50*(7), 783–859.

Binder, K. (2012). *Monte Carlo and molecular dynamics simulations in polymer science*. Oxford University Press.

Bray, A. J. (1994). Theory of phase-ordering kinetics. *Advances in Physics, 43*(3), 357–459.

Cahn, J. W., & Hilliard, J. E. (1958). Free energy of a nonuniform system. I. Interfacial free energy. *The Journal of Chemical Physics, 28*(2), 258–267.

Cahn, J. W., & Hilliard, J. E. (1959). Free energy of a nonuniform system. III. Nucleation in a two-component incompressible fluid. *The Journal of Chemical Physics, 31*(3), 688–699.

Frenkel, D., & Smit, B. (2002). *Understanding molecular simulation: From algorithms to applications* (2nd ed.). Academic Press.

Furukawa, H. (1985). A dynamic scaling assumption for phase separation. *Advances in Physics, 34*(6), 703–750.

Hansen, J.-P., & McDonald, I. R. (2013). *Theory of simple liquids* (4th ed.). Academic Press.

Hoover, W. G. (1985). Canonical dynamics: Equilibrium phase-space distributions. *Physical Review A, 31*(3), 1695–1697.

Jones, J. E. (1924). On the determination of molecular fields. II. From the equation of state of a gas. *Proceedings of the Royal Society A, 106*, 463–477.

Laradji, M., Guo, H., Grant, M., & Zuckermann, M. J. (1997). Molecular dynamics study of spinodal decomposition in binary fluids. *Physical Review E, 55*(5), 5455–5460.

Lifshitz, I. M., & Slyozov, V. V. (1961). The kinetics of precipitation from supersaturated solid solutions. *Journal of Physics and Chemistry of Solids, 19*(1–2), 35–50.

Lorentz, H. A. (1881). Ueber die Anwendung des Satzes vom Virial in der kinetischen Theorie der Gase. *Annalen der Physik und Chemie, 248*, 127–136.

Martyna, G. J., Klein, M. L., & Tuckerman, M. (1992). Nosé–Hoover chains: The canonical ensemble via continuous dynamics. *The Journal of Chemical Physics, 97*(4), 2635–2643.

Nosé, S. (1984). A unified formulation of the constant temperature molecular dynamics methods. *The Journal of Chemical Physics, 81*(1), 511–519.

Onuki, A. (2002). *Phase transition dynamics*. Cambridge University Press.

Puri, S., & Wadhawan, V. (Eds.). (2009). *Kinetics of phase transitions*. CRC Press.

Rapaport, D. C. (2004). *The art of molecular dynamics simulation* (2nd ed.). Cambridge University Press.

Siggia, E. D. (1979). Late stages of spinodal decomposition in binary mixtures. *Physical Review A, 20*(2), 595–605.

Stauffer, D., & Aharony, A. (1994). *Introduction to percolation theory* (2nd ed.). Taylor & Francis.

Swope, W. C., Andersen, H. C., Berens, P. H., & Wilson, K. R. (1982). A computer simulation method for the calculation of equilibrium constants for the formation of physical clusters of molecules: Application to small water clusters. *The Journal of Chemical Physics, 76*(1), 637–649.

Velasco, E., & Toxvaerd, S. (1994). Molecular dynamics simulation of phase separation in binary Lennard–Jones mixtures. *Molecular Physics, 81*(6), 1295–1310.

Verlet, L. (1967). Computer experiments on classical fluids. I. Thermodynamical properties of Lennard–Jones molecules. *Physical Review, 159*(1), 98–103.

Wagner, C. (1961). Theorie der Alterung von Niederschlägen durch Umlösen (Ostwald-Reifung). *Zeitschrift für Elektrochemie, 65*, 581–591.